Physics of Plasmas

RESEARCH ARTICLE | FEBRUARY 16 2023

Theory of ion holes in plasmas with flat-topped electron distributions

Harikrishnan Aravindakshan ; Ivan Y. Vasko ; Amar Kakad ; Bharati Kakad ; Rachel Wang

Phys. Plasmas 30, 022903 (2023)
https://doi.org/10.1063/5.0086613

Physics of Plasmas ARTICLE scitation.org/journal/php

Theory of ion holes in plasmas with flat-topped electron distributions

Cite as: Phys. Plasmas **30**, 022903 (2023); doi: 10.1063/5.0086613
Submitted: 27 January 2022 · Accepted: 15 January 2023 ·
Published Online: 16 February 2023

Harikrishnan Aravindakshan,[1,a)] Ivan Y. Vasko,[2,3] Amar Kakad,[1] Bharati Kakad,[1] and Rachel Wang[2,4]

AFFILIATIONS

[1]Indian Institute of Geomagnetism, New Panvel, Navi Mumbai 410218, India
[2]Space Sciences Laboratory, University of California at Berkeley, Berkeley, California 94720, USA
[3]Space Research Institute of Russian Academy of Sciences, Moscow 117997, Russia
[4]Department of Physics, University of California at Berkeley, Berkeley, California 94720, USA

[a)]Author to whom correspondence should be addressed: hari1501@gmail.com

ABSTRACT

Coherent bipolar electric field structures with negative unipolar potentials are widely observed in space plasmas. These bipolar structures are often found to be ion Bernstein Greene Kruskal (BGK) modes or ion holes. Most theoretical models of ion holes assume them to be stationary with respect to the background plasma that follows either Maxwellian or kappa-type distribution. In this paper, we present a new theoretical model of ion holes where the structures are non-stationary, and electrons follow flat-topped distribution. We use the classical BGK approach to derive the inequality separating allowed and forbidden simultaneous values of amplitude and spatial width of ion holes. The model reveals that the parametric space for the existence of ion holes decreases with their speed. We applied the developed model to the largest available dataset of ion holes obtained from the magnetospheric multiscale spacecraft observations in the Earth's bow shock region.

I. INTRODUCTION

Numerous spacecraft have observed a single or train of isolated electrostatic structures with the bipolar parallel electric field in space plasma environments.[1–8] They are interpreted as electron phase-space holes,[9–11] i.e., solitary waves with positive electrostatic potential formed in a nonlinear stage of various electron streaming instabilities[12–16] or ion phase-space holes,[6,7,17] i.e., solitary waves of negative electrostatic potential formed due to ion streaming instabilities.[6,7] Recently, Magnetospheric Multiscale Mission (MMS) reported the observation of bipolar electrostatic structures with negative electrostatic potentials in the Earth's bow shock region.[5–7] These structures were interpreted as ion phase-space holes or ion holes (IHs).

The ion or electron phase-space holes are generally addressed as Bernstein Greene Kruskal (BGK) modes.[18–23] One can use the Sagdeev pseudopotential approach,[24,25] studied extensively by Schamel, or an integral solution approach to study BGK modes.[18,19] In the pseudopotential approach, the trapped and passing particle distribution function is assumed, and the Poisson equation is solved to obtain the potential.[26–28] In the integral solution approach, the BGK approach, the form of the potential and the passing particle distribution, is assumed. They are plugged into the Poisson equation and obtain the trapped density, which can be expressed as an integral of the trapped particle distribution function. Thus, from the solution of this integral equation, we obtain the trapped particle distribution function.[19,20,29,30] In this study, we use the integral solution approach to model the ion BGK modes.

Recently, Vasko *et al.*[4] and Wang *et al.*[6,7] have reported thousands of the bipolar electric field structures with negative unipolar potential in the Earth's bow shock region. A detailed analysis by Wang *et al.*[7] has shown that the observed structures cannot be solitons of any type, because the structures with larger spatial scales tend to have larger amplitudes, while in the case of solitons we would observe the opposite trend.[31] Thus, they interpreted these structures in terms of BGK ion holes. The majority of the theoretical models are incapable of explaining these observations due to the theoretical restrictions on the ion-to-electron temperature ratio. However, Aravindakshan *et al.*[22,23] have recently proposed the model for ion holes, which is applicable to any case of the ion-to-electron temperature ratio.

Most theoretical models of ion holes assume that these structures are stationary, and the background plasma follows either Maxwellian or kappa-type distribution. In this paper, we present a theory of non-stationary ion holes in a plasma where electrons follow flat-topped type distribution and ions follow drifting Maxwellian distribution. The paper is arranged as follows. Section II presents the theoretical model, Sec. III discusses the numerical results, Sec. IV discusses the application of the model to the ion hole observations in the Earth's bow shock, and the paper ends with concluding remarks in Sec. V.

II. THEORETICAL MODEL

We consider plasma consisting of electrons and ions, wherein the ions follow drifting Maxwell distribution and electrons follow flat-topped distribution function. Due to any plasma process, let us assume that a coherent bipolar electrostatic structure has been produced. Its bipolar electric field is associated with a unipolar Gaussian electrostatic potential with negative polarity. The electrostatic potential of the bipolar structure is Φ, and the velocity of the structure in the rest frame of background ions is U_s. The spatial coordinate x is measured in units of the electron Debye length λ_D, the velocities are in units of $(2T_e/m_i)^{1/2}$, and the normalized electrostatic potential is $\varphi = e\Phi/T_e$, while $M = U_s/(2T_e/m_i)^{1/2}$ is the Mach number. Here, T_e is the temperature of electrons, m_i is the mass of ions, and the denominator $(2T_e/m_i)^{1/2}$ is roughly comparable to the ion sound speed. Here, the ion hole is assumed to propagate with velocity U_s with respect to ions and electrons, which will help us to understand the non-stationary effects of ion holes. From an observational standpoint, MMS measures the ion hole velocity, U_s^*, and the plasma flow velocity, $\mathbf{V_i}$, in the spacecraft rest frame. For the analysis, we convert it into the rest frame of the plasma ions using the formula, $U_s = |U_s^* - \hat{\mathbf{k}} \cdot \mathbf{V_i}|$. Here, $\hat{\mathbf{k}}$ is the unit vector along the ion hole propagation direction. Now, this speed (U_s) is further used to compute the Mach number in the plasma rest frame.[7]

We consider the following form of the flat-topped distribution function as the unperturbed electron velocity distribution function:[32,33]

$$F_0(v^2/v_0^2) = \frac{n_0 C_{n\zeta}}{v_0}\left[1 + \left(\frac{v^2}{v_0^2}\right)^n\right]^{-\zeta}, \tag{1}$$

where n_0 is the equilibrium density, ζ is the spectral index, n is the factor that controls the flatness of the distribution function, v_0 is a scale velocity related to the electron thermal velocity, $(2T_e/m_e)^{1/2}$, as given in Eq. (3), and $C_{n\zeta}$ is the normalization constant defined as

$$C_{n\zeta} = \frac{\Gamma(\zeta)}{2\Gamma\left(1+\frac{1}{2n}\right)\Gamma\left(\zeta - \frac{1}{2n}\right)}. \tag{2}$$

The pictorial representation of the flat-topped distribution function is given in Fig. 1. The top left panel shows the case of $\zeta = 1$ and top right panel shows the case of $\zeta = 2$. The bottom left panel shows the case of $\zeta = 4$ and bottom right panel shows the case for $\zeta = 9$. The solid lines represented by different colors shows the case for different values of n. The dashed cyan colored line represents the case for Maxwell–Boltzmann distribution function. The flat-topped electron distribution function has two essential factors, n and ζ, which control its shape. Here, n controls the flatness of the distribution function, whereas ζ controls the height of the distribution function. The flatness of the distribution function commonly influences the average thermal energy of the electrons.

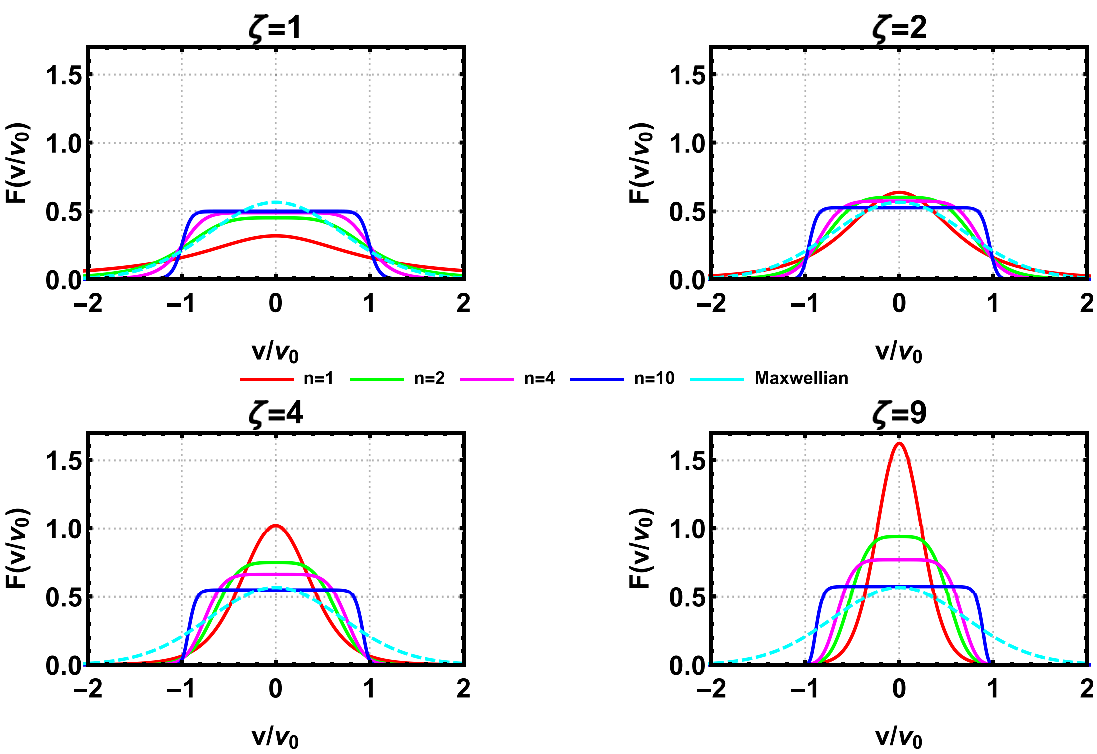

FIG. 1. The figure shows the form of flat-topped electron distribution function for various spectral indices. The dashed curve in cyan color represents the Maxwell–Boltzmann distribution function. Here, for the case of flat-topped distribution, we have used v_0 as normalization factor and in the case of Maxwellian, the velocity is normalized with $v_{th,e}$.

The relation between the electron temperature and parameter v_0 is

$$T_e = m_e v_0^2 \frac{B(\zeta - 3/2n, 3/2n)}{B(\zeta - 1/2n, 1/2n)} \equiv m_e v_0^2 f_{n\zeta}. \tag{3}$$

Here, $B(x, y)$ is the Beta function defined as

$$B(x, y) = \frac{\Gamma(x)\Gamma(y)}{\Gamma(x+y)}.$$

In the presence of the bipolar electric field structure, the electron distribution function adjusts to the electrostatic potential. As a result, in the Eq. (1) we substitute, $v^2 \rightarrow v^2 - 2e\varphi/m_e$,

$$F_e(v, x) = F_0(v^2/v_0^2 - 2e\varphi/m_e v_0^2). \tag{4}$$

Using the relation Eqs. (3) and (4), we determined the perturbed density of electrons as

$$F_e(v, x) = F_0(v^2/v_0^2 - 2f_{n\zeta}\varphi). \tag{5}$$

The perturbed density of electrons is determined as

$$n_e(\varphi) = \int_{-\infty}^{+\infty} F_0(v^2/v_0^2 - 2f_{n\zeta}\varphi)dv.$$

We can expand this into the series up to terms of φ^2 under the assumption of small amplitude expansion, and the electron density is given by

$$n_e(\varphi) = 1 + a_1\varphi + a_2\varphi^2, \tag{6}$$

where

$$a_1 = 2\zeta f_{n\zeta} C_{n\zeta} B(\zeta + 1/2n, 1 - 1/2n), \tag{7}$$

$$a_2 = -f_{n\zeta}^2 C_{n\zeta} \zeta B(\zeta + 3/2n, 1 - 3/2n). \tag{8}$$

The asymptotic expansion is valid everywhere at $n > 1$ except a vicinity of $n = 3/2$. Clearly, at $n > 3/2$, we have $a_2 > 0$, while at $n < 3/2$, we have $a_2 < 0$.

The bipolar electric field is associated with a unipolar electrostatic potential with negative polarity, which can typically be approximated by a Gaussian profile. Even though the assumption that the potential conforms to a Gaussian profile is an over-simplification for the observed scenarios, this approximation by a Gaussian function will not significantly alter the results relative to what would be obtained for any other more realistic functional forms. Moreover, the use of a Gaussian profile will simplify the mathematical formulation. Thus, the potential can be written as

$$\varphi = -\psi \exp(-x^2/2\delta^2), \tag{9}$$

where ψ is the maximum amplitude of the potential and δ is the width of the potential.

Therefore, $\partial^2\varphi/\partial x^2$ can be expressed as a function of φ as follows:

$$\rho(\varphi) = \frac{\partial^2\varphi}{\partial x^2} = \frac{\varphi}{\delta^2}\left[2\ln\left(\frac{\psi}{\varphi}\right) - 1\right]. \tag{10}$$

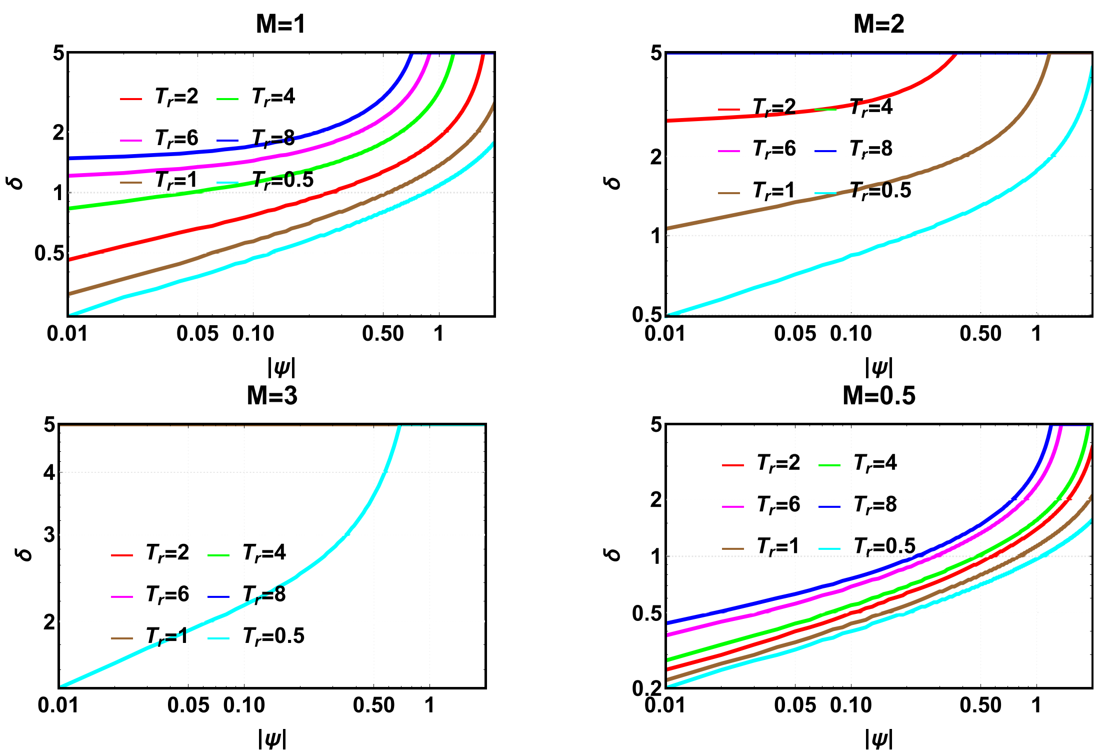

FIG. 2. The effect of Mach number and ion-to-electron temperature ratio, $T_r = (T_i/T_e)$ on the physically plausible ψ–δ region for the existence of IHs is shown here for $n = 4$ and $\zeta = 1$. Different colored lines are used to represent the effect of temperature ratio. The area above each curve defines the plausible ψ–δ region of existence of IHs.

The above-mentioned normalization results in the Poisson equation

$$\frac{\partial^2 \varphi}{\partial x^2} = n_e - n_p - n_{tr}, \tag{11}$$

where n_e and n_p are perturbations of electron density and density of ions on passing orbits. The trapped ion density, n_{tr}, is

$$n_{tr}(\varphi) = \int_{\varphi}^{0} \frac{f_{tr}(w)}{\sqrt{\varphi - w}} dw. \tag{12}$$

Here, w is the total energy variable defined as $w = v^2 - \varphi$. The distribution function is defined in the region $-\psi < w < 0$. The density n_p of ions of the passing ions is

$$n_p(\varphi) = \int_0^{\infty} \frac{f_p^{(+)}(w) + f_p^{(-)}(w)}{2(w-\varphi)^{1/2}} dw. \tag{13}$$

Here, $f_p(w)$ is the passing ion distribution function. The velocity distribution functions of passing ions (with $w > 0$) is

$$f_p^{(\pm)}(w) = \frac{1}{\sqrt{\pi T_r}} \exp\left[-\frac{\left(M \pm \sqrt{w}\right)^2}{T_r}\right], \tag{14}$$

where $T_r = T_i/T_e$. Thus, $f_p(w)$ can be written as

$$f_p(w) = \frac{f_p^{(+)}(w) + f_p^{(-)}(w)}{2}.$$

Thus, the distribution function of trapped ions is

$$f_{tr}(w) = -\frac{1}{\pi}\frac{d}{dw}\left[\int_w^0 \frac{n_e(\varphi) - n_p - \rho(\varphi)}{\sqrt{\varphi - w}} d\varphi\right]. \tag{15}$$

Now all we need is to calculate the trapped ion distribution. The distribution function of the trapped ions is defined at $-\psi < w < 0$ and can be determined as follows:

$$f_{tr}(w) = -\frac{1}{\pi}\frac{d}{dw}\left[\int_w^0 \frac{n_e(\varphi) - n_p(\varphi) - \rho(\varphi)}{\sqrt{\varphi - w}} d\varphi\right]. \tag{16}$$

By substituting, Eqs. (6), (10), and (13) in Eq. (16), we obtain the trapped ion distribution function. The distribution function of trapped ions $f_{tr}(w)$ can be split into three parts $f_{tr} = f_{tr}^{(1)}(w) + f_{tr}^{(2)}(w) + f_{tr}^{(3)}(w)$, which each $f_{tr}^{(i)}$ corresponding to n_e, n_p, and $\rho(\varphi)$, respectively. The detailed computations show that

$$f_{tr}^{(1)}(w) = -\frac{2\sqrt{-w}}{\pi}\left[a_1 + \frac{4}{3}a_2 w\right], \tag{17}$$

$$f_{tr}^{(2)}(w) = \frac{I\left(\sqrt{-w/T_r}, -M/\sqrt{T_r}\right) + I\left(\sqrt{-w/T_r}, M/\sqrt{T_r}\right)}{\pi^{3/2}\sqrt{T_r}}, \tag{18}$$

$$f_{tr}^{(3)}(w) = \frac{2\sqrt{-w}}{\pi\delta^2}\left[2\ln\left(\frac{\psi}{4w}\right) + 1\right]. \tag{19}$$

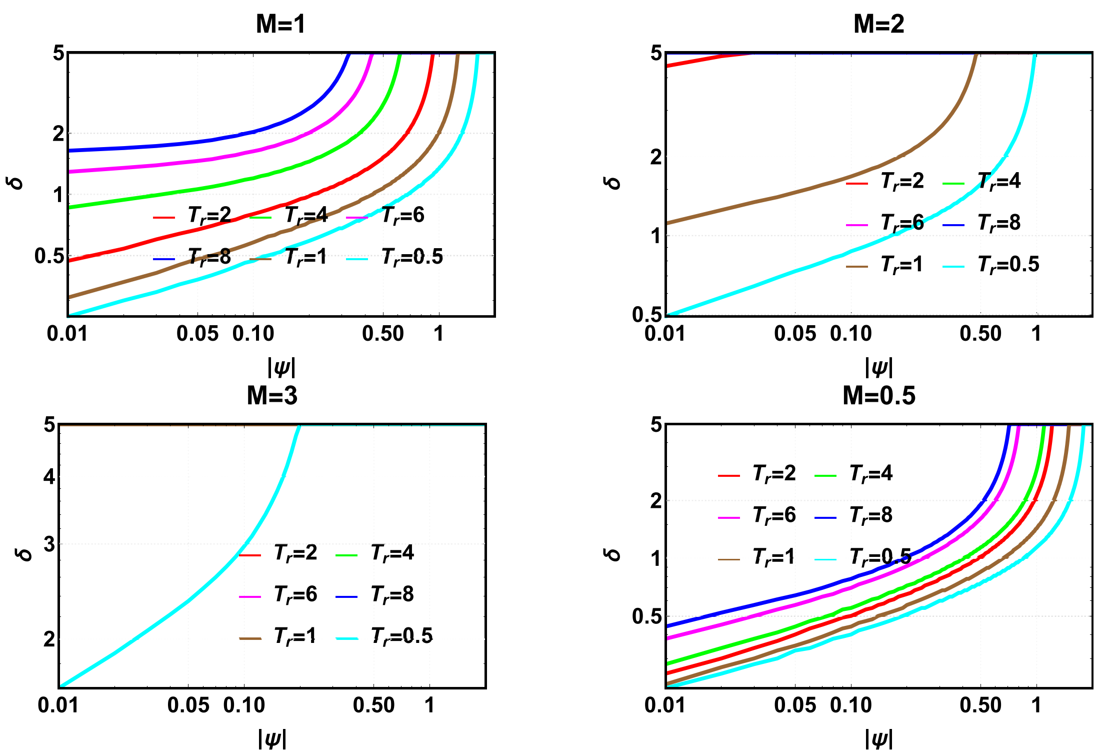

FIG. 3. The effect of Mach number and ion-to-electron temperature ratio, $T_r = (T_i/T_e)$ on the physically plausible region for the existence of IHs is shown here for $n = 2$ and $\zeta = 2$. Different color schemes are used to represent the effect of temperature ratio and different subplots show the effect of Mach number.

In the above-mentioned equations,

$$I(\alpha, \beta) = \int_0^{\infty} \frac{e^{-(\alpha x+\beta)^2}}{1+x^2} dx. \tag{20}$$

The summation of Eqs. (17)–(19) describe the total distribution function of trapped ions. However, the integral in Eq. (18) can only be calculated numerically when the $M > 0$. When we calculate the total distribution function, $f_{tr}(w)$ numerically, we arrive at a relation defined by the width and amplitude of the potential that helps to understand the structure the wave potential that can sustain an ion hole equilibria.

III. NUMERICAL RESULTS

Assuming the positivity of the trapped ion distribution function defined in Eqs. (17)–(19), we derive a parametric space defined by the width (δ) and amplitude (ψ) of the potential, which supports the existence of IHs. Other than the factors, n and ζ, there are parameters like Mach number, M, temperature ratio, T_i/T_e, which play a significant role in determining the $\delta - \psi$ parametric space that support existence of IHs. We discuss these aspects in detail by considering the following two cases:

A. Case I: $n=4$, $\zeta=1$

Figure 2 shows the width–amplitude relation for $n = 4$ and $\zeta = 1$. Each subplot describes the case of different Mach numbers, and each

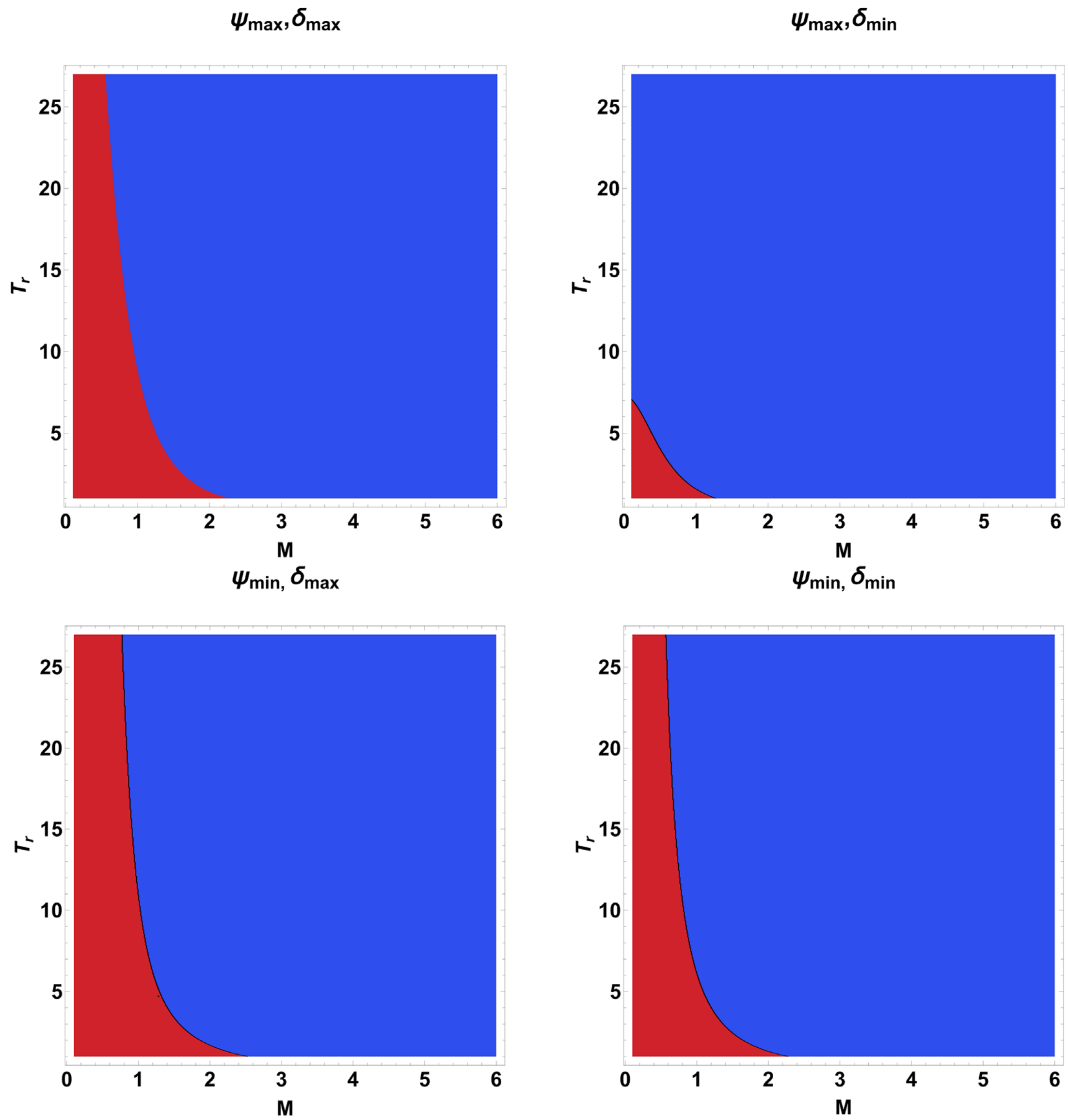

FIG. 4. The variation in temperature ratio with the Mach number for different observed ψ and δ is given. The red region represents the allowed region and the blue region denotes the restricted region for IHs. Here, the values of n and ζ are assumed as 4 and 1, respectively.

line in the subplot describes case for different temperature ratios. The space above each curve represents the set of ψ and δ that can support physically plausible IHs. As the region above the curve decreases with the increasing Mach number, the allowed combination of width and amplitude to support physically plausible IH equilibrium decreases. We can see that for $M = 0.5$ (see bottom right panel in Fig. 2) and 1 (see top left panel in Fig. 2), all the temperature ratios support IHs. However, as the Mach number increases like we see in the top right panel and bottom left panel in Fig. 2, the physically plausible solutions are obtained only for lower temperature ratios. Moreover, as the temperature ratio decreases, the region that the inequality satisfies increases; for a constant Mach number. Thus, the ion holes are more favorable when the electron temperature is larger than the ion temperature.

B. Case II: $n=2, \zeta=2$

Figure 3 describes the variation of the width–amplitude region for different Mach number and temperature ratio T_r, for $n = 2$ and $\zeta = 2$. Each subplot describes the case of different Mach numbers, and each line in the subplot describes the temperature ratio assumed. In this case, the overall trend remains the same as mentioned in the case I. Nevertheless, it is essential to note some significant changes regarding the allowed width–amplitude parameter space of the IHs; especially, in the case of higher Mach numbers. In the case of higher Mach numbers, $M = 2$ and $M = 3$ (compare the top right panel and bottom left panel in Figs. 2 and 3), it can be observed that the allowed region defined by the width (δ) and amplitude (ψ) of the potential is significantly smaller. This implies that when the electrons follow distribution function more closer to flat-topped distribution function, the system can support IHs that moves with a greater speed. As the "flatness" decreases with the decrease in n and the increase in ζ (see Fig. 1), the system is less likely to support IHs with large velocity.

IV. APPLICATION TO MMS OBSERVATIONS OF ION HOLES

In this section, we apply our theoretical model to the largest dataset of ion holes, reported by Wang *et al.*,[7] where more than 2000 ion holes were observed. For each observed ion hole, Wang *et al.*[7] determined the spatial scale, amplitude, and velocity. Figure 4 displays the relation between temperature ratio and Mach number that divides the parameter space into allowed and restricted regions for the existence of IHs. The red region represents the allowed region and the blue region shows the restricted region of IHs. The theoretical regions in terms of T_r and M are shown here for four different combinations of maximum and minimum observed values of ψ and δ from Wang *et al.*[7] It can be seen that the allowed region is larger, when the δ is large, compared to the other combinations.

Now, we compare the theoretical prediction of IHs with the actual ion hole observations. In Fig. 5, the theoretically allowed combinations of M and T_r are shown. As mentioned in the case of Fig. 4, the red colored region shows the allowed combinations of M and T_r and blue region shows the restricted combinations. The Mach numbers and temperature ratios of the observed IHs are superimposed on the theoretical values and are shown with the yellow dots. The Mach numbers of the observed IHs are defined here exactly the way we defined in the theory, i.e., $M = U_s/(2T_e/m_i)^{1/2}$. We assumed the maximum observed values of ψ and δ ($\psi = -0.52$ and $\delta = 54.2$) to generate this plot. Moreover, we have also assume $n = 4$ and $\zeta = 1$ in this plot. Figure 5 shows that

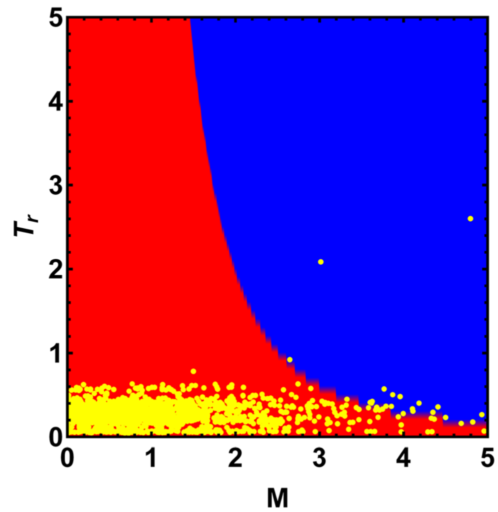

FIG. 5. The variation in temperature ratio with the Mach number for the maximum observed values of ψ and δ is given. The red region represents the allowed region and the blue region denotes the restricted region. Here, the values of n and ζ are assumed as 4 and 1, respectively. The yellow dots indicate the temperature ratio and Mach number of the observed ion holes by MMS spacecraft.

the theoretically allowed region of ion holes does not exist for higher Mach numbers and higher temperature ratios temperature ratios, as predicated by the theory (see Figs. 2 and 3). It can be seen that majority of the observations fits well with the theory. However, there are some observations IHs whose the parameters fall in the theoretically restricted region. This might be due to the use of single Maxwellian ion distribution function that does not accurately describe the ion distributions. This is certainly expected, because the ion distribution function in the bow shock is in general, a combination of incoming more or less Maxwellian solar wind ions and a population of reflected protons. As these reflected protons can have different distribution, the total velocity distribution of ions will be a combination of different distributions. The modeling of such combination is rather complicated, because the distributions are agyrotropic and might be highly non-Maxwellian. Nevertheless, the use of Maxwellian model shows that the majority (98%) of the ion holes are in the region allowed by the theory. According to our model, we try to say that if the relative velocity of the structure is larger, then the probability of system to support an ion hole is less. As most of the IH observations still fall within the theoretically allowed region, the present theory can be applied to model IH observations, where the electrons follows the flat-topped or close to flat-topped distribution.

V. CONCLUSIONS

The theoretical model for ion holes in space plasma where the electrons follow flat-topped distribution function was developed, incorporating the ion hole velocity. In this paper, we have discussed about the effects of various parameters (both electrons and ions) on the existence of ion holes in a collisionless plasma. Such effects were studied by observing the parametric spaces defined by width and amplitude of the wave potential, Mach number, and temperature ratio. The theoretical analysis showed that with the increase in Mach number and temperature ratio, the probability for the existence of IHs decreases. The parametric space defined by Mach number and temperature ratio also demonstrates that if the assumed width of the wave potential is large and the amplitude is small, such a combination favors the IHs existence the most. On the other hand, if the assumed width of the wave potential is small and the amplitude is large, such a combination favors the IHs existence the least. Another important factor is the role of the shape of electron distribution in the existence of ion holes. The model shows that the shape of electron distribution (which is controlled by n and ζ) has greater impacts on the width–amplitude region that supports IHs when the structure is moving at a higher speed and has a higher temperature ratio. The theoretical analysis shows that the electron distribution with a more flat-top shape in the system favors IHs even if they move at high velocities.

Finally, we applied our theory to the largest ion hole dataset obtained from MMS observations in the Earth's bow shock region and found that majority of the observations falls within the theoretically allowed region, thus providing a validation of our theory.

ACKNOWLEDGMENTS

The work of I.V. and R.W. was supported by NASA Heliophysics Guest Investigator (Grant No. 80NSSC21K0730).

AUTHOR DECLARATIONS

Conflict of Interest

The authors have no conflicts to disclose.

Author Contributions

Harikrishnan Aravindakshan: Conceptualization (equal); Project administration (equal); Formal analysis (lead); Methodology (equal); Writing – original draft (lead); Writing – review & editing (equal). **Ivan Vasko**: Conceptualization (equal); Writing – review & editing (equal); Formal analysis (supporting); Methodology (equal). **Amar Kakad**: Conceptualization (equal); Project administration (equal); Writing – review & editing (equal); Formal analysis (equal); Methodology (equal); **Bharati Kakad**: Conceptualization (equal); Formal analysis (supporting); Writing – review & editing (equal). **Rachel Wang**: Conceptualization (equal); Formal analysis (supporting), Writing – review & editing (supporting).

DATA AVAILABILITY

The data used in this study are open and available in the following link https://lasp.colorado.edu/mms/sdc/public/about/browse-wrapper/

REFERENCES

[1]H. Matsumoto, H. Kojima, T. Miyatake, Y. Omura, M. Okada, I. Nagano, and M. Tsutsui, Geophys. Res. Lett. **21**, 2915, https://doi.org/10.1029/94GL01284 (1994).

[2]S. D. Bale, P. J. Kellogg, D. E. Larsen, R. P. Lin, K. Goetz, and R. P. Lepping, Geophys. Res. Lett. **25**, 2929, https://doi.org/10.1029/98GL02111 (1998).

[3]A. Kakad, B. Kakad, C. Anekallu, G. Lakhina, Y. Omura, and A. Fazakerley, J. Geophys. Res. **121**, 4452, https://doi.org/10.1002/2016JA022365 (2016).

[4]I. Y. Vasko, R. Wang, F. S. Mozer, S. D. Bale, and A. V. Artemyev, Front. Phys. **8**, 156 (2020).

[5]I. Vasko, F. Mozer, V. Krasnoselskikh, A. Artemyev, O. Agapitov, S. Bale, L. Avanov, R. Ergun, B. Giles, P.-A. Lindqvist *et al.*, Geophys. Res. Lett. **45**, 5809 https://doi.org/10.1029/2018GL0778357 (2018).

[6]R. Wang, I. Vasko, F. Mozer, S. Bale, A. Artemyev, J. Bonnell, R. Ergun, B. Giles, P.-A. Lindqvist, C. Russell *et al.*, Astrophys. J. Lett. **889**, L9 (2020).

[7]R. Wang, I. Y. Vasko, F. S. Mozer, S. D. Bale, I. V. Kuzichev, A. V. Artemyev, K. Steinvall, R. Ergun, B. Giles, Y. Khotyaintsev, P. A. Lindqvist, C. T. Russell, and R. Strangeway, J. Geophys. Res. **126**, e2021JA029357 https://doi.org/10.1029/2021JA029357 (2021).

[8]B. Kakad, A. Kakad, H. Aravindakshan, and I. Kourakis, Astrophys. J. **934**, 126 (2022).

[9]Y. Tong, I. Vasko, F. Mozer, S. D. Bale, I. Roth, A. Artemyev, R. Ergun, B. Giles, P.-A. Lindqvist, C. Russell *et al.*, Geophys. Res. Lett. **45**, 11513–11519, https://doi.org/10.1029/2018GL079044 (2018).

[10]A. Lotekar, I. Vasko, F. Mozer, I. Hutchinson, A. Artemyev, S. Bale, J. W. Bonnell, R. Ergun, B. Giles, Y. V. Khotyaintsev *et al.*, J. Geophys. Res. **125**, e2020JA028066, https://doi.org/10.1029/2020JA028066 (2020).

[11]F. Mozer, O. Agapitov, B. Giles, and I. Vasko, Phys. Rev. Lett. **121**, 135102 (2018).

[12]Y. Omura, H. Matsumoto, T. Miyake, and H. Kojima, J. Geophys. Res. **101**, 2685, https://doi.org/10.1029/95JA03145 (1996).

[13]K. Pommois, F. Valentini, O. Pezzi, and P. Veltri, Phys. Plasmas **24**, 012105 (2017).

[14]M. Gedalin, Geophys. Res. Lett. **26**, 1239, https://doi.org/10.1029/1999GL900239 (1999).

[15]N. Shimada and M. Hoshino, Phys. Plasmas **11**, 1840 (2004).

[16]J. Büchner and N. Elkina, Phys. Plasmas **13**, 082304 (2006).

[17]J. McFadden, C. Carlson, R. Ergun, F. Mozer, L. Muschietti, I. Roth, and E. Moebius, J. Geophys. Res. **108**, 8018, https://doi.org/10.1029/2002JA009485 (2003).

[18]I. B. Bernstein, J. M. Greene, and M. D. Kruskal, Phys. Rev. **108**, 546 (1957).

[19]H. Aravindakshan, A. Kakad, and B. Kakad, Phys. Plasmas **25**, 052901 (2018).

[20]H. Aravindakshan, A. Kakad, and B. Kakad, Phys. Plasmas **25**, 122901 (2018).

[21]I. H. Hutchinson, Phys. Plasmas **24**, 055601 (2017).

[22]H. Aravindakshan, P. H. Yoon, A. Kakad, and B. Kakad, Mon. Not. R. Astron. Soc. **497**, L69 (2020).

[23]H. Aravindakshan, A. Kakad, B. Kakad, and P. H. Yoon, Plasma **4**, 435 (2021).

[24]R. Z. Sagdeev and A. Galeev, *Nonlinear Plasma Theory* (WA Benjamin, 1969).

[25]A. Gurevich, Sov. Phys. JETP **26**, 575 (1968), see http://jetp.ras.ru/cgi-bin/dn/e_026_03_0575.pdf

[26]H. Schamel, Plasma Phys. **13**, 491 (1971).

[27]S. Bujarbarua and H. Schamel, J. Plasma Phys. **25**, 515 (1981).

[28]H. Schamel, Phys. Scr. **1982**, 228.

[29]L.-J. Chen, "Bernstein-Greene-Kruskal solitary waves in collisionless plasma," Ph.D. dissertation (University of Wash, Seattle, 2002).

[30]V. Turikov, Phys. Scr. **30**, 73 (1984).

[31]R. Sagdeev, Rev. Plasma Phys. **4**, 23 (1966), see https://books.google.be/books?id=VCwIzgEACAAJ

[32]L. B. Wilson III, L.-J. Chen, S. Wang, S. J. Schwartz, D. L. Turner, M. L. Stevens, J. C. Kasper, A. Osmane, D. Caprioli, S. D. Bale *et al.*, Astrophys. J. Suppl. Ser. **243**, 8 (2019).

[33]L. B. Wilson, L.-J. Chen, S. Wang, S. J. Schwartz, D. L. Turner, M. L. Stevens, J. C. Kasper, A. Osmane, D. Caprioli, S. D. Bale *et al.*, Astrophys. J. Suppl. Ser. **245**, 24 (2019).